Microstructural evolutions and mechanical properties of transient liquid phase bonded WC-Co/St52 with BNi-2 interlayer

Abstract

In this study, the transient liquid phase bonding of St52 plain carbon steel to WC-Co compound using BNi-2 interlayer with a thickness of 50 μm was investigated. For this purpose, samples were bonded at a temperature of 1050 °C and holding times of 1, 15, 30 and 45 min. After the joining process, the microstructure of the bonded samples was examined using a scanning electron microscope equipped with energy-dispersive X-ray spectroscopy. X-ray diffraction analysis was also used to investigate the effects of bonding parameters on the phase transformations of the bonding region. Microhardness and tensile shear tests were also conducted to study the mechanical properties of the bonded samples. Microstructural studies showed that the formation mechanism of the solidification zone in all samples was isothermal solidification mechanism. The results of the investigations showed that the only phase in the isothermal solidification zone was the nickel base solid solution. The maximum hardness in all samples belonged to WC-Co base materials due to the presence of WC particles in it. The maximum tensile-shear strength was related to the sample with bonding time of 30 min. The mode of failure in all samples was a combination of brittle and ductile fracture.

Keywords: Transient liquid phase bonding, St52 steel, WC-Co compound, Microstructure, Mechanical properties

1. Introduction

New work systems with harsh conditions require a combination of materials of different natures, which are challenging to join with each other. The joining of ceramics and cermets to

metal alloys combines the properties of these two groups of materials, i.e., the hardness, wear, and heat resistance of ceramics and cermets, and the toughness and ductility of metals. Various joining methods, including brazing [1], gas tungsten arc welding [2], laser beam welding [3], electron beam welding [4], oxyacetylene welding [5], friction welding [6], and diffusion bonding [7, 8], can be used to join these materials. Sometimes it is even possible to join ceramics and cermets to metal alloys with a combination of these processes.

Tungsten-cobalt carbide (WC-Co) is a group of cemented carbides that consists of different amounts of tungsten carbide and cobalt. The simultaneous presence of tungsten carbide and cobalt in this group of cemented carbides causes high strength and wear resistance due to the presence of tungsten carbide and appropriate ductility and toughness due to the presence of cobalt. In fact, this group of cemented carbides is a type of composite material in which tungsten carbide particles are dispersed in the cobalt matrix [9]. Of course, it should be mentioned that due to the expensive and brittle nature of these materials, their application has been limited. One solution to overcome these problems is to join this group of cemented carbides to alloys including steels [10].

One of the processes that can be used to join WC-Co to different steel groups is the transient liquid phase (TLP) bonding process. The TLP bonding process is a very suitable choice due to the ability to create high-strength bonding between materials with different chemical compositions and mechanical properties. In the TLP bonding process, a thin interlayer (pure metal or alloy) is used for the joining process. With the melting of this interlayer and the interactions that occur in the bonding region, the base materials are joined to each other.

One of the biggest challenges in the dissimilar joining of materials is the lack of sufficient mechanical strength of the bonding. In this type of bonding, due to the different chemical composition of the base materials and the mismatch of their thermal expansion coefficient, residual stresses are created at the joining region, which causes a decrease in the bonding strength [11]. One of the advantages of using the TLP bonding process is the control and reduction of residual stresses in the bonding region compared to other joining methods, especially fusion joining processes.

As mentioned, various joining processes such as diffusion bonding, friction stir welding, laser and electron beam, and even gas tungsten arc welding have been used to join WC-Co to different steel grades. Li et al. [8] joined WC-11Co to steel by a diffusion bonding process using a nickel base interlayer. The reason for the use of the nickel interlayer in TLP was to prevent the direct bonding of steel and WC-11Co. With the use of a nickel interlayer, the formation of brittle intermetallic compounds in the joint region is significantly reduced. In this

case, the diffusion of Fe towards the WC-Co base material and its reaction with C and W are prevented, and the formation of the η phase is minimized. As well, because the nickel interlayer is ductile, it can reduce the destructive effects of residual stresses caused by phase mismatch and the difference in thermal expansion coefficients of steel and WC-11Co. Yin et al. [12] also used laser beam welding with the Fe-Ni Invar interlayer with different thicknesses for dissimilar bonding of WC-Co and steel. They stated that a metallurgical bond without defects and cracks between 316L stainless steels and WC-Co can be achieved by increasing the thickness of the interlayer. Because in such a case, the interlayer can act as a buffer between the WC-Co base material and the melting zone.

Yu et al. [3] also used fiber laser welding with Fe-Ni Invar interlayer for dissimilar bonding of WC-Co and steel. They stated that the maximum bending strength of the created joint was 980 MPa, which was obtained at a laser power of 3 kW, a scanning speed of 0.024 m/s and an input energy of 125 J/mm and there are phases such as austenite, martensite, WC, Fe_3W_3C and Co_6W_6C in the bonding region. Cheniti et al. [13] also used the friction welding method to create dissimilar joining of the WC-Co/AISI 304L. They created this joint with and without using NiCr interlayer. The results of their investigations showed that the interdiffusion of elements caused the creation of different zones in the joint region, which is aggravated by the use of NiCr interlayer. They stated that when using the NiCr interlayer, the formation of a nickel-cobalt solid solution is strengthened, and this prevents the formation of a brittle intermetallic phase at the bonding region. The maximum shear strength reported by them was about 512 MPa.

According to the studies, there is limited information about joining different types of WC-Co cermets to different grades of steels using the TLP bonding process. Therefore, the purpose of this research is to use and expand the TLP bonding process in the joining of these two materials by using the TLP bonding process and BNi-2 interlayer. Also, considering the creation of St 52/Cu/WC-Co bonding using the TLP bonding process in a previous study [14], another goal of this research is to compare the shear strength of the created bonding using Cu and BNi-2 interlayers.

2. Experimental procedures

In this research, St52 and WC-10 Co samples with dimensions of 5×10×10 mm^3 were joined to each other by the TLP bonding process using a 50 μm thickness BNi-2 amorphous interlayer. The chemical composition of the BNi-2 interlayer is presented in Table 1. To perform the bonding process, the mating surfaces of the samples were sanded using silicon carbide paper up to number 1000 and then polished. After that, the samples were washed in the acetone bath

for 15 min by an ultrasonic machine. Finally, the interlayers were placed between the two samples of St52 and WC-10 Co, and the joining sets were created as WC-10Co/BNi-2/St52. A fixture was used to fix the joining sets and also to apply pressure to them. The joining process was carried out in a vacuum furnace (10^{-3} Pa) at a temperature of 1050 °C with holding times of 1, 15, 30 and 45 min. The furnace heating rate was chosen to be 10 °C/min. After the bonding process, the cross sections of the samples were prepared perpendicular to the bonding surface using standard metallographic methods. Microstructural studies were carried out using a scanning electron microscope (SEM, FEI ESEM QUANTA 200) equipped with an energy-dispersive X-ray spectroscopy. X-ray diffraction analysis (XRD, Philips X'pert pro) was also used to investigate the phase transformation in the bonding region due to the bonding process. The microhardness tester under the load of 100 g and dwell time of 10 s was used to measure the microhardness distribution through the bonding regions. Tensile-shear tests were also performed to measure the strength of the produced joints with strain rate of 2 $mm.min^{-1}$. Then, in order to determine the failure mode of the samples, the fracture surfaces obtained from the tensile-shear tests were examined using SEM.

Table 1 Chemical composition of BNi-2 interlayer

Elements	Fe	Cr	Si	C	B	Ni
wt.%	3	7	4.5	0.06	3.2	Bal.

3. Results and discussion

3.1. Microstructural evolutions

The SEM images of the produced joint at 1050 °C with a holding time of 1 min using the BNi-2 interlayer are shown in Fig. 1. According to this figure, it is clear that there are no porosities, cracks, or discontinuities in the created joint. Therefore, it can be said that a proper bonding between the base materials was established. During the TLP bonding process, as the temperature increases and it reaches the melting point of the interlayer, the interlayer begins to melt, and after completely melting, the base material dissolves in the molten phase until the thermodynamic equilibrium is created between the molten phase and the base materials. After the equilibrium is established, the diffusion of melting point depressant agents takes place and the solidification phenomenon of the molten phase begins, which can be done in two ways, isothermal and athermal, based on the selected parameters of the process, especially

temperature and time [15]. The interdiffusion between the molten interlayer and the solid phases (base materials) and the decrease in the concentration of the melting point depressant agents cause the activation of the isothermal solidification mechanism [16, 17]. But if the parameters of the process are selected in such a way that there is not enough time to complete isothermal solidification, the remaining melt in the centerline of the joint is solidified based on another mechanism called the athermal solidification mechanism. Under such conditions, the remaining melt is solidified in the form of the eutectic structure by cooling the joint set from the joining temperature to lower temperatures. So, the driving force for the activation of the athermal solidification mechanism is the cooling of the remaining molten phase [18]. The microstructure of the athermal solidification zone generally includes brittle and hard phases. These brittle compounds are formed due to the eutectic reaction between the melting point depressant elements and the main alloying elements in the interlayer. Therefore, the presence of these phases with eutectic structure are the main features of this zone [19].

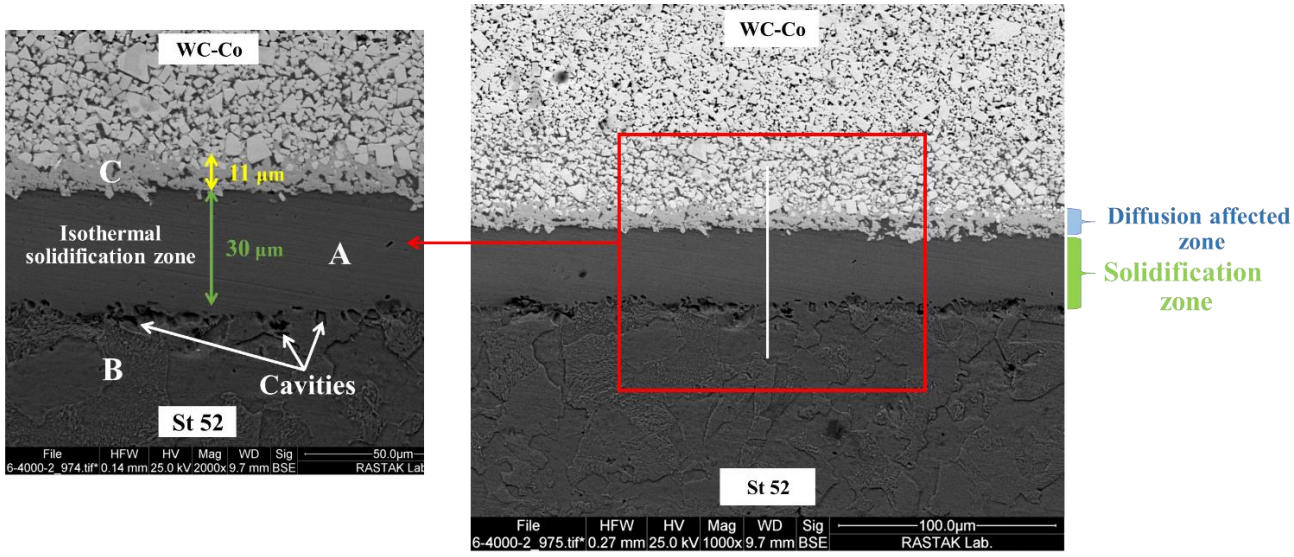

Fig. 1. SEM images of the created joint at 1050 °C with holding time of 1 min using BNi-2 interlayer.

As is clearly seen in Fig. 1, the solidification zone of the created joints between WC-Co and St52 base materials in the centerline of the joint is free of any eutectic and intermetallic compounds. This means that the solidification zone was only formed based on the isothermal solidification mechanism, and the athermal solidification mechanism was not activated. This is despite the fact that usually in TLP bonding, processes are performed in low holding times, such as 1 min; the solidification region consists of two isothermal solidification zones in the

vicinity of the base materials and an athermal solidification zone in the centerline of the joint [18, 19].

According to the Hume-Rothery rules, if the difference in the atomic radius of two interacting elements is less than 15%, the possibility of forming a solid solution is more than forming intermetallic compounds. Based on the Hume-Rothery rules, iron, nickel, cobalt and chromium elements are preferably present as solid solutions in the structure. Meanwhile, the affinity of boron with other elements, especially with chromium, is high. Therefore, the probability of forming boride compounds is higher than other compounds in the joint structure. One of the reasons for the lack of an athermal solidification zone can be attributed to the low heating rate of the furnace. Due to the low heating rate of the furnace and the increase in the time it takes for the furnace temperature to reach the temperature of the joining process, enough time is provided for the interdiffusion of the elements, and considering that boron has a high diffusion coefficient, it quickly diffused into the base material, so the amount of boron remaining at the joint was not enough to lead to the formation of boride compounds. Therefore, isothermal solidification is completed in lower times.

SEM/EDS elemental analysis was used to investigate the elemental changes in the joint region and suggest the phases that were created as a result of the jointing process in the joint region. The result of SEM/EDS analysis of the isothermal solidification zone shown in Fig. 1 with the symbol A, is presented in Table 2. According to the amount of nickel in the isothermal solidification zone of the created joint using the BNi-2 interlayer, it can be said that this zone is rich of nickel element. Also, the richness of the isothermal solidification zone with the nickel element in Fig. 2, which is related to the linear elemental analysis of the path shown by the white line in Fig. 1, can be clearly seen. Also, other elements such as Si, W, Co and Cr are present in the isothermal solidification zone. A point that should be pointed out is that some of these elements were not present in the initial chemical composition of the interlayer. This means that these elements enter from the base materials to the molten interlayer and finally the isothermal solidification due to the interdiffusion phenomenon. By examining the distribution of the mentioned elements in the isothermal solidification zone (Fig. 3), it can be said that these elements are completely and uniformly distributed in this zone. Therefore, according to performed analyses and according to the microstructure images, it can be suggested that the only phase in the isothermal solidification zone is a nickel base solid solution (γ-NiSS). Other researchers also reported the formation of this phase in the isothermal solidification zone. Pouranvari et al. [20] reported the formation of such a phase in the isothermal solidification zone in the TLP bonding process of Inconel 718 using the BNi-2 interlayer. Baharzadeh et al.

[21] also stated that in the dissimilar joining of Inconel X-750 to dual-phase stainless steel using the BNi-3 interlayer, a nickel base solid solution was formed in the isothermal solidification zone.

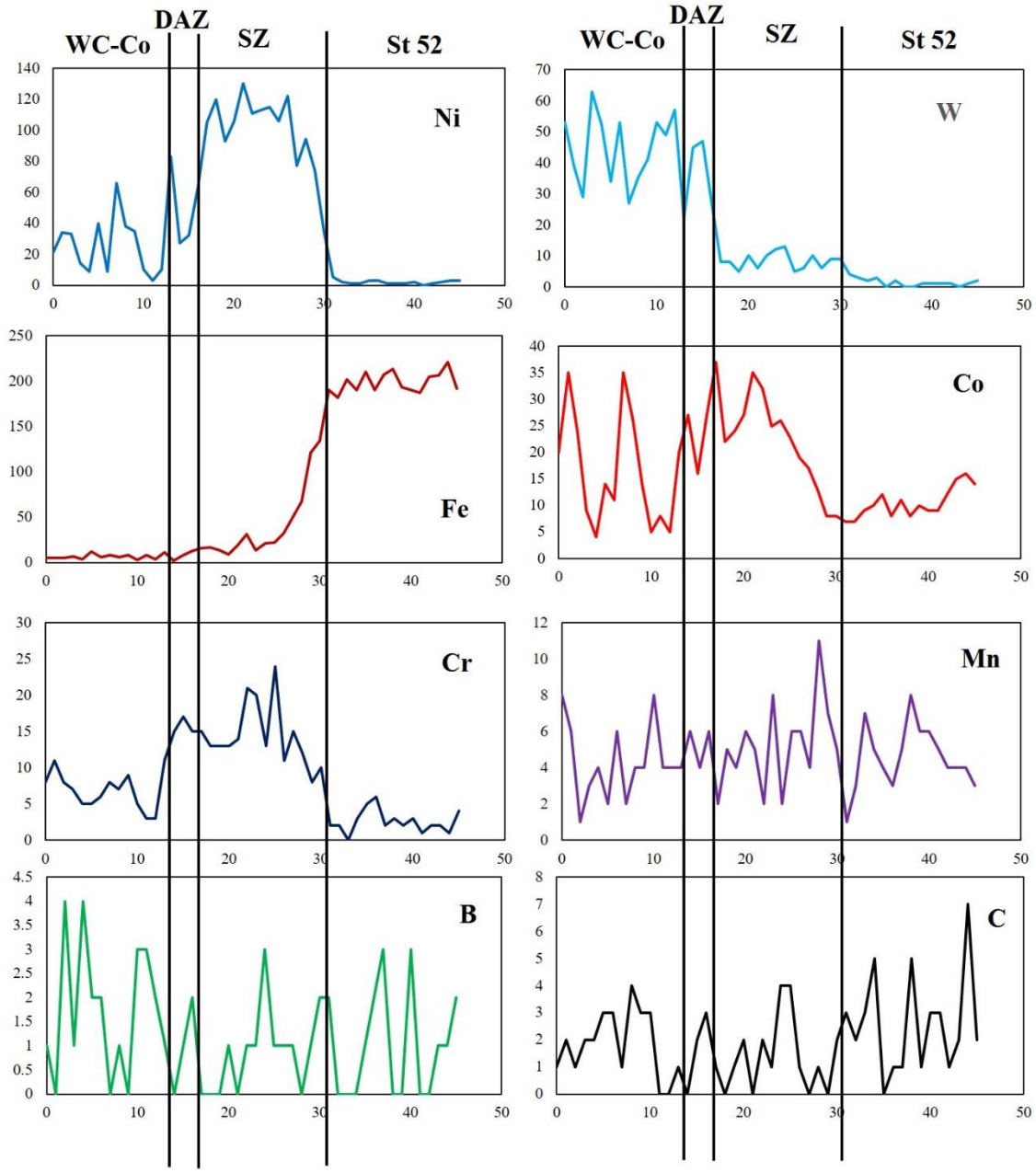

Fig. 2. Linear elemental analysis of the path shown by the white line in Fig. 1

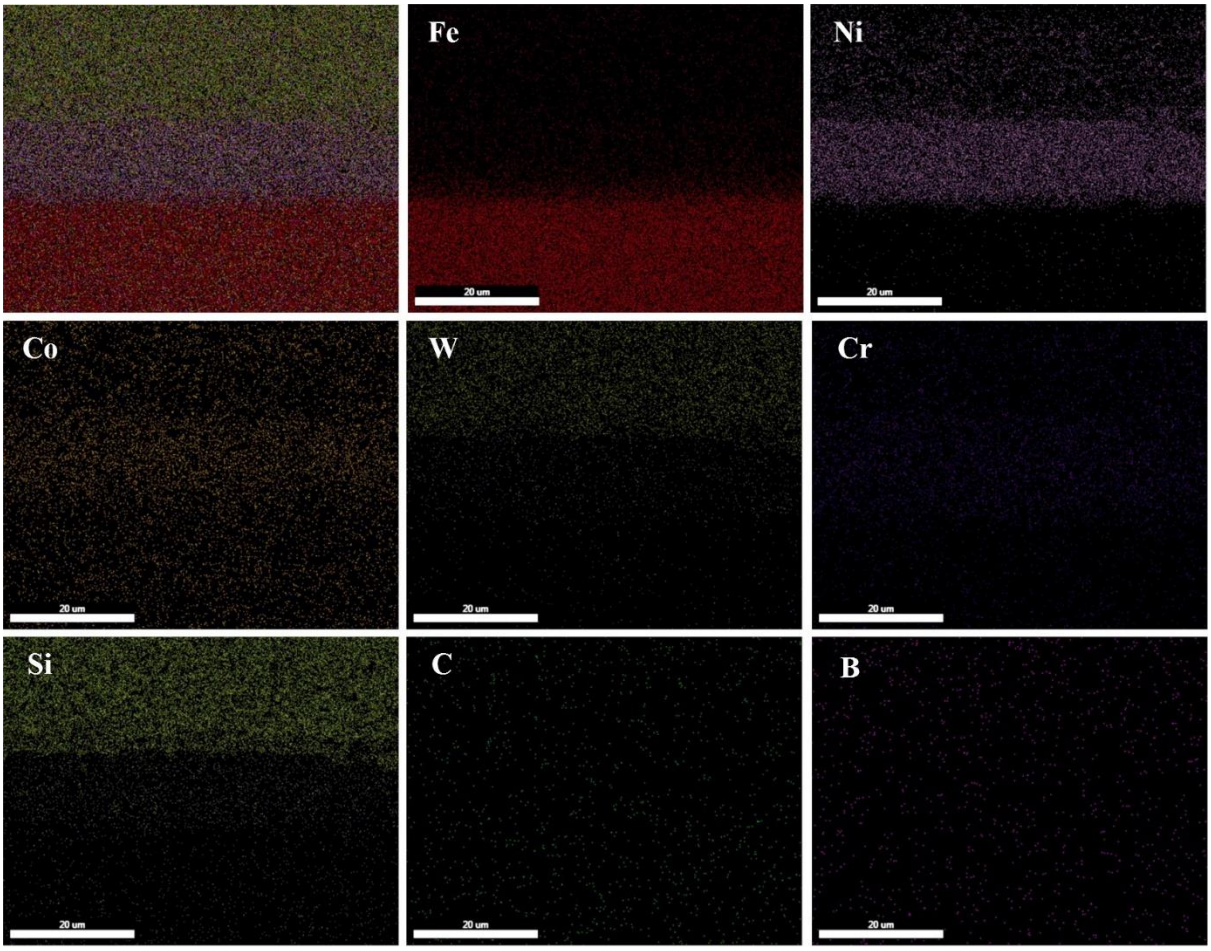

Fig. 3. Elemental map analysis of the bonded sample at temperature of 1050 °C with holding time of 1 min.

Table 2 The results of SEM/EDS analysis of the points marked in Fig. 1.

Point	Chemical composition (at.%)								Suggested phase
	Fe	Ni	Co	W	Mn	Cr	Si	B	
A	5.89	65.07	14.11	1.86	0.83	4.94	6.83	0.47	γNi SS
B	95.71	0.91	0.77	0.27	1.21	0.49	0.53	0.11	Fe SS
C	3.76	24.15	21.07	32.86	1.19	9.74	6.70	0.53	ηPhase S

Considering that isothermal solidification is carried out with the diffusion of melting point depressant agents from the molten interlayer towards the base materials, therefore, the diffusion of these agents into the base materials causes changes in the interface between the isothermal solidification zone and the base materials, and the diffusion-affected zone, which its microstructure is influenced by diffusion and the type of melting point depressant agents, is formed. The difference between this zone and the base materials is the creation of secondary phase precipitates [22]. According to the SEM image of the bonding region at a temperature of 1050 °C and holding time of 1 min shown in Fig. 1, it should be stated that there are no

secondary phase compounds on the St52 base metal side. Based on the elemental analysis of point B shown in Fig. 1 and that reported in Table 2, it can be said that due to the interdiffusion between the interlayer and the steel base metal, only the chemical composition of this zone underwent a slight change, and no secondary phase was formed in this zone. This is while in the research conducted by other researchers, the existence of this zone has been reported on the steel base metal side. Baharzadeh et al. [21] in TLP of Inconel X-750 to 2205 dual-phase stainless steel using the BNi-2 interlayer reported the formation of secondary phase compounds such as Cr-rich borides and the creation of the diffusion-affected zone in the steel base metal side. The non-formation of secondary phase precipitates and the non-creation of the diffusion-affected zone in the St52 base metal side can be attributed to the low heating and cooling rate of the furnace. As mentioned, secondary phase compounds form as a result of the reaction of melting point depressant agents during cooling from high to lower temperatures. As the temperature decreases, the amount of these elements exceeds the solubility limit in the base metal, and therefore, the insolubility of the melting point depressant agents in the base material causes them to combine with other alloying elements, and the diffusion-affected zone forms. When the heating and cooling rates of the furnace are low, the diffusional melting point depressant agents have enough time to diffuse to regions far away from the interface. Considering that the amount of the melting point depressant elements, which is boron in the present study, is limited, therefore, its diffusion to regions far away from the interface causes the amount of boron to not exceed its solubility limit in iron during cooling and so be present as a solution in the Fe crystal lattice. Therefore, dissolved B in iron cannot react with other existing alloy elements and cannot create secondary phase compounds, and therefore the diffusion zone affected is not formed.

Another point that should be mentioned is the presence of a number of cavities in the interface between the isothermal solidification zone and the steel base metal. Some reasons for the presence of these cavities can be stated. One of the reasons for the presence of these cavities is the difference in the thermal expansion coefficient between the interlayer and the base metals. Also, due to the presence of microscopic distortions on the surface of the interlayer and the surface of the base materials, an air gap is created between the interlayer and the base material in the assembled set joint, and therefore some air is trapped in this gap that cannot be discharged and creates cavities [23]. Another reason for the formation of cavities in the interface can be attributed to the difference in the diffusion coefficient of various elements in the bonding region. Due to the difference in the diffusion coefficient of different elements in the interface of the base material and the interlayer, the diffusion rate of the elements is different and this

causes the cavities to form in the part where the diffusion rate of the elements is higher. These types of cavities are called Kirkendall cavities [24].

On the opposite side, as shown in Fig. 1, the diffusion-affected zone of the WC-Co base material side is created as a dark gray band along the interface of the WC-Co base material and the isothermal solidification zone. According to chemical composition analysis of this zone, which is reported in Table 2 (point c), it can be said that the created phase in this zone is the brittle intermetallic η phase. Regarding the formation mechanism of the η phase, it should be noted that the η phase is poor from carbon and contains less C and W and more Fe, Co and Ni than the WC phase. As the temperature increases and reaches the joining process temperature, some WC particles are decomposed. Decomposition of the WC particles makes cobalt rich from carbon element. Therefore, a carbon concentration gradient is created in the joining system. On the side of the WC-Co base material, the carbon concentration is high, and on the side of the steel base material, the carbon concentration is low. This difference in carbon element concentration creates a concentration gradient. Therefore, carbon tends to move from the side of the WC-Co base material to the side of the steel base material through the created molten phase during the joining process. In this case, cobalt becomes poor from carbon and this factor causes the decomposition of a larger amount of WC. But due to the fact that the rate of decomposition of WC is lower than the rate of diffusion of C, the equilibrium between C and W in cobalt is lost. On the other hand, due to the concentration gradient, iron and nickel also move from the steel base material side and the interlayer to the WC-Co base material and diffuse into it. So, a carbon-poor environment is created on the WC-Co base material side in the Fe (Co, Ni)-W-C system. This carbon-poor environment causes the formation of the η phase [4]. In the phase diagram presented in Fig. 4, the low carbon region that leads to the formation of the η phase in the Co-W-C ternary system can be seen [25].

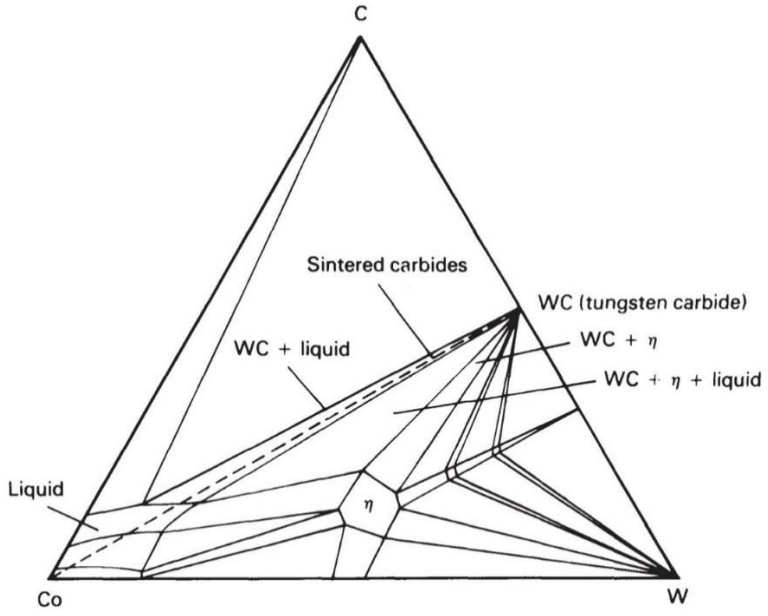

Fig. 4. Cobalt-tungsten-carbon ternary phase diagram [25].

Another point that should be mentioned is the absence of boride compounds in the diffusion-affected zone of WC-Co base material. The lack of formation of boride compounds can be attributed to the creation of the η phase in this zone. The formation of the η phase in the form of a narrow band along the interface between the isothermal solidification zone and the WC-Co base material creates a barrier against boron diffusion from the interlayer to the WC-Co base material [26].

In order to investigate the effect of time on the properties and microstructure of the bonded samples at 1050 °C, the joining process was also performed at holding times of 15, 30 and 45 min in addition to the 1 min. The SEM images of the created joint at the mentioned times are shown in Fig. 5. As it is clear in these images that the increase in time caused changes in the bonding region.

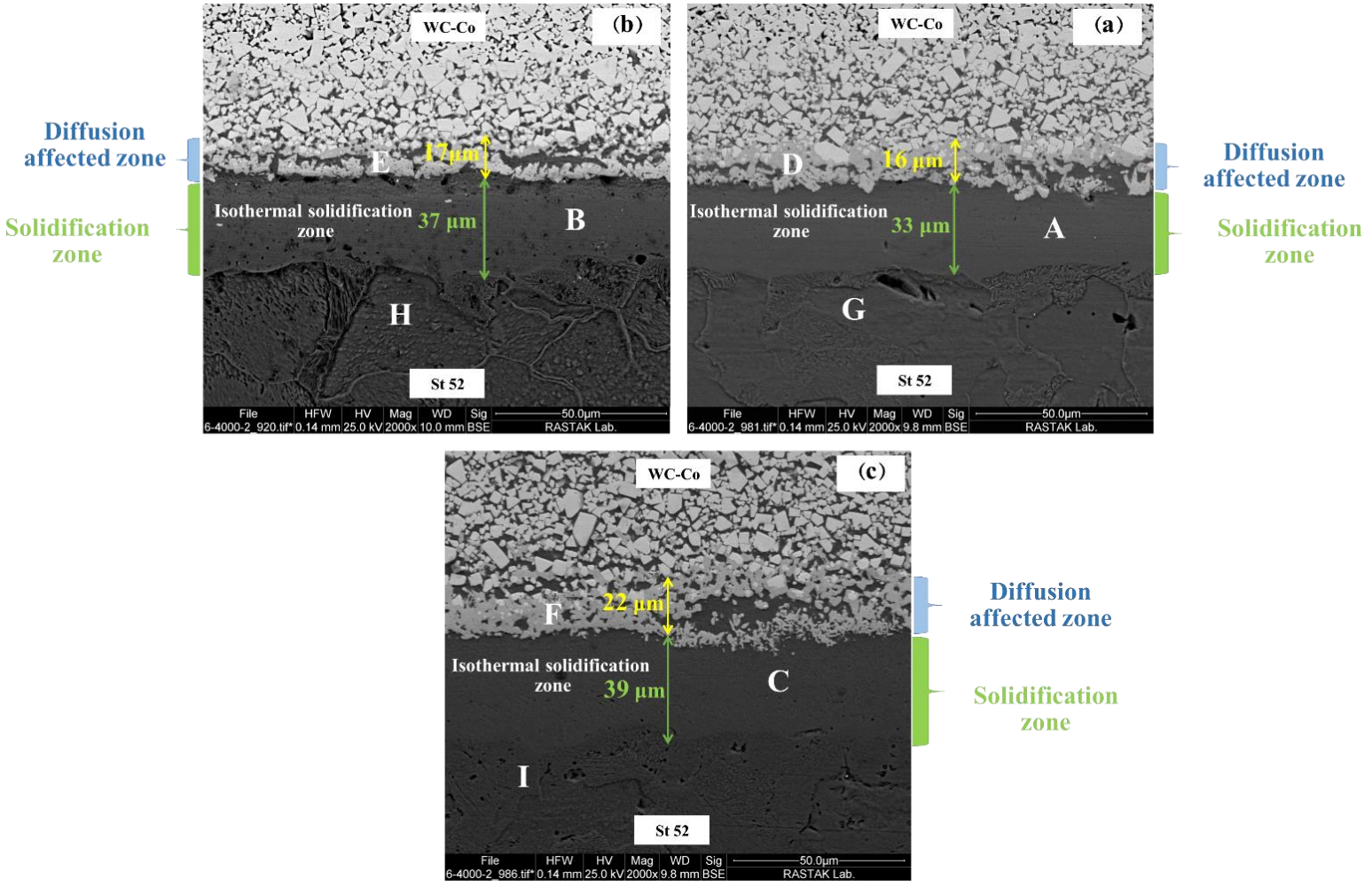

Fig. 5 SEM images of the bonded samples using BNi-2 interlayer at 1050 °C and holding times of a: 15, B: 30, and C: 45 min.

In Fig. 5, the width changes of the solidification zone of the created joints at 1050 °C and holding times of 15, 30, and 45 min can be seen. According to Fig. 5, it is clear that the width of the isothermal solidification zone increased with the increase of the holding time at a constant temperature. The reason for this can be attributed to the higher interdiffusion of elements in longer holding times and the increase in the volume of the melt phase in the joint region with the increase in holding time [27-29]. Also, based on the results of the SEM/EDS analysis reported in Table 3 from the isothermal solidification zones at different holding times, which are shown in Fig. 5 with letters A, B, and C, it is clear that in these zones, no phase transformation has occurred due to the increase in holding time, and the only phase present in these zones is the nickel base solid solution. But as it is clear from the results of the analysis presented in Table 3, with the increase of holding time, the amount of nickel in the isothermal solidification zone decreased and the amount of other alloy elements, especially iron, increased.

This issue expresses the increase of alloying elements interdiffusion with the holding time between the molten interlayer and the base material, especially the steel base material. One of the reasons that there was less interdiffusion between the interlayer and the WC-Co base material could be attributed to the creation of a narrow band of η phase at the interface between the interlayer and the WC-Co base material. This created a narrow band at the interface that can act as a barrier and prevent the interdiffusion of elements between these two zones [26].

Table 3 Chemical analysis (at.%) of the marked points in Fig. 5

Point	Chemical composition (at.%)								Suggested phase
	Fe	Ni	Co	W	Mn	Cr	Si	B	
A	23.13	57.71	8.29	1.73	0.85	5.13	2.68	0.48	γNi SS
B	25.82	53.89	8.51	1.61	0.94	4.36	3.97	0.90	γNi SS
C	32.92	50.52	6.87	1.37	0.97	3.69	3.22	0.44	γNi SS

Also, according to Fig. 5, it can be clearly recognized that the width of the diffusion-affected zone of the WC-Co base material has been increased. As it is clear in Figs. 1 and 5, with the increase of the processing time from 1 to 45 min at a constant temperature of 1050 °C, the width of the diffusion-affected zone of the WC-Co base material increased. According to the analysis of the marked points with the letters D, E, and F in Fig. 5, which are presented in Table 4 and are respectively related to the diffusion-affected zone of the WC-Co base material, the bonded samples at 15, 30, and 45 min, it should be mentioned that the only phase available in these zones is the η phase. As mentioned in the previous sections, the formation of the η phase depends on the decomposition of WC, the diffusion and lack of carbon, and the re-reaction of these elements with other alloy elements. These mentioned items depend on the time and temperature of the process. By increasing the time of the process at a constant temperature, the necessary time is provided for the further decomposition of WC, and this causes the volume of the η phase to increase; therefore, the width of the diffusion-affected zone was also increased with the increase of time.

Table 4 Chemical composition (at.%) of the points marked on Fig. 5

Point	Chemical composition (at.%)								Suggested phase
	Fe	Ni	Co	W	Mn	Cr	Si	B	
D	4.20	23.27	20.71	29.70	2.13	11.88	7.59	0.52	phase η
E	3.77	25.30	26.42	26.40	1.73	8.22	7.18	0.98	phase η
F	2.76	20.49	26.06	35.98	1.02	4.60	8.52	0.57	phase η

It should be noted that on the side of the steel base metal, by increasing the holding time to 15, 30, and 45 min, the secondary phase compounds were not formed in the diffusion-affected zone like the sample with a holding time of 1 min. As mentioned earlier, the diffusion of boron to areas far from the interface between the isothermal solidification zone and the steel base metal and the reduction of boron concentration at the interface and lower concentration of it than the solubility limit of boron in solid iron can be the reasons for this issue. However, it should be pointed out that based on the SEM/EDS analysis performed on the steel base material at different times, the results are reported in Table 5, with the increase in the time of the process, the presence of alloying elements such as cobalt and nickel in the steel base material increased due to rising the interdiffusion by increasing the time. On this basis, the concentration of Co and Ni elements increased from 0.77 and 0.91 to 1.61 and 1.36 at.%, respectively, with the increase of the process time from 1 to 45 min.

Table 5 Chemical composition (at.%) of the points marked on Fig. 5

Point	Chemical composition (at.%)								Suggested phase
	Fe	Ni	Co	W	Mn	Cr	Si	B	
G	94.96	0.52	1.09	0.43	1.49	0.65	0.56	0.30	Fe SS
H	94.40	0.97	1.52	0.51	1.51	0.64	0.33	0.12	Fe SS
I	93.03	1.36	1.61	0.68	1.47	0.81	0.43	0.61	Fe SS

It should also be mentioned that the cavities that were present at the interface of the isothermal solidification zone and the steel base metal in the bonded sample at the holding time of 1 min, were not present in the bonded samples at higher times and were removed. The increase in time improves the wettability of the created molten phase in the bonding region, and the atomic diffusion also increases, and this causes the cavities to fill and decrease [23].

3.2. Mechanical properties

3.2.1. Microhardness

The microhardness profile obtained from the cross-section of a bonded sample is a reliable method of assessing the homogeneity of the microstructure. The microhardness profile is a quantitative measurement of the mechanical properties of different joint zones and is a suitable indicator of microstructure changes in the joint region. Microhardness profile can be used to evaluate the effect of newly created phases in the joint region on mechanical properties [20, 30].

Fig. 6 illustrates the microhardness changes of the created joint region using the BNi-2 interlayer at 1050 ℃ for holding times of 1 and 45 min. This hardness profile reflects the

mechanical properties of the produced joints. Hardness decreases from WC-Co base material to steel base metal in all joints, as shown in Fig. 6. By matching the hardness profile with the corresponding microstructure images of these two samples, which are shown in Figs. 1 and 5 (c), it can be concluded that the hardness profile, like the joint region, is based on hardness changes, and it is divided into several zones. In fact, the hardness changes in the microhardness profile are due to the microstructural variation in the joint region.

According to the hardness profile related to the produced joint using the BNi-2 interlayer at 1050 °C for 1 min as shown in Fig. 6, it is clear that the hardness of the WC-Co base material is around 1000 HV. A decreasing trend in hardness is observed when moving from the WC-Co base material to the joint region. It is worth noting that the hardness of the diffusion-affected zone of the WC-Co base material side is nearly identical to the hardness of the base material. This is because of the development of hard and continuous η phase in this zone. Therefore, the process of decreasing hardness starts by entering the isothermal solidification zone and continues continuously until reaching the steel base metal. Therefore, the isothermal solidification zone has a lower hardness compared to the WC-Co base metal and its diffusion-affected zone. This is due to the high inherent hardness of WC and the presence of the η phase in these areas.

The isothermal solidification zone also shows a higher hardness than the steel base metal. The increased hardness in the isothermal solidification zone can be explained by the higher inherent hardness of nickel compared to iron. Additionally, the interaction of the alloying elements in the base materials contributes to this effect by the creation of a solid solution hardening mechanism that further hardens the zone. According to the analysis of the chemical composition of this zone presented in Table 2 (point A), it is clear that elements such as iron, cobalt, chromium, and silicon have diffused into this zone from the base materials and increased the hardness of this zone by the solid solution hardening mechanism. By passing through the isothermal solidification zone and entering the steel base material, the hardness decreases to about 250 HV. The isothermal solidification zone also shows a higher hardness than the steel base metal. The increased hardness in the isothermal solidification zone can be explained by the higher inherent hardness of nickel compared to iron. A point that should be pointed out is that a slight hardness gradient can be seen from the interface of the isothermal solidification zone and the steel base material to the areas further away from the interface. The reason for this can be attributed to the interdiffusion of the elements from the interlayer into the steel base material. For example, the initial concentration of nickel in the steel base material was 0%, while by performing the joining operation at a holding time of 1 min according to the

results that are presented in Table 2 (point B), it is clear that the concentration of nickel in the steel base material increased to about 1%. Also, based on the results, it is clear that other elements, such as cobalt and tungsten, diffused into the steel base material. The same issue caused a slight increase in the hardness of the steel base metal near its interface with the solidification zone at the same temperature compared to the zones further away from it. Such a trend was also observed in the hardness changes in the TLP bonding created between the WC-Co material and the steel base material using a copper interlayer [14].

Also, the hardness of the produced joint using the BNi-2 interlayer at the temperature of 1050 °C and holding time of 45 min can be seen in Fig. 6. As it is clear in this figure, the trend of hardness changes in this sample is similar to the bonded sample at 1 min and a decrease in hardness can be seen by moving from WC-Co base material to steel base material. As mentioned earlier, these changes are related to the microstructural changes in the joint region and the trend of hardness changes is similar to the hardness changes of the bonded sample at 1 min.

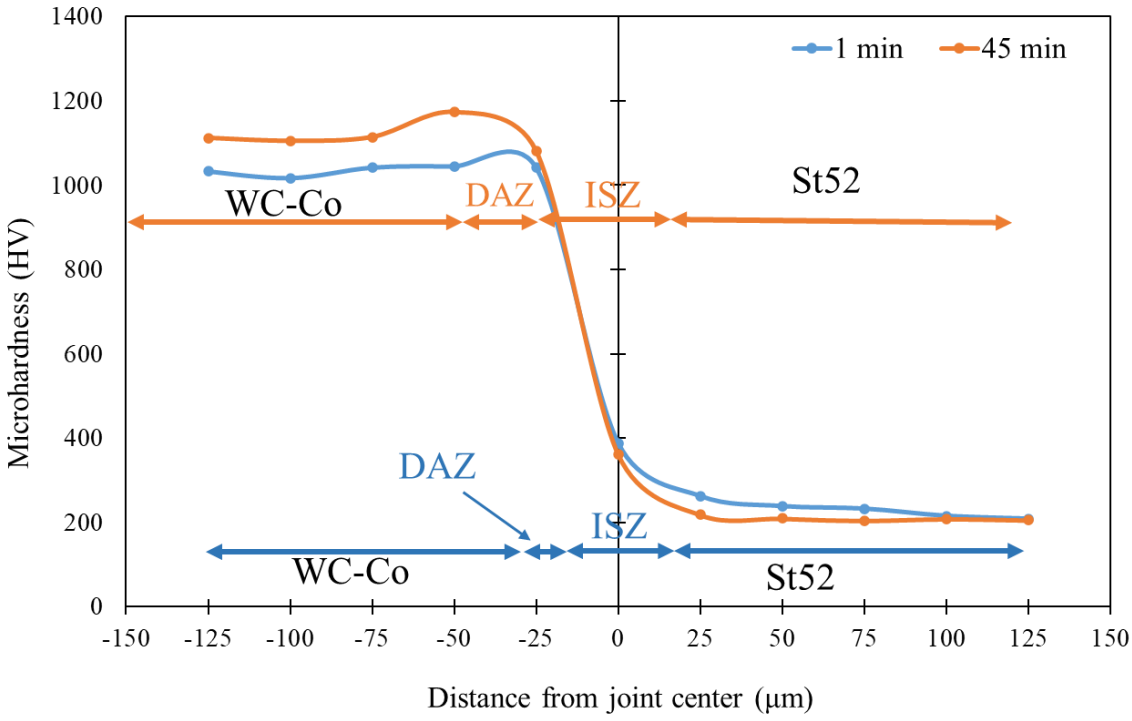

Fig. 6. Changes in the microhardness of the bonded sample at 1050 °C with BNi-2 interlayer with holding times of 1 and 45 min.

3.2.2. Shear strength of the joints

In the tensile shear strength test, shear stress is locally applied to the bonding region. By using this test, it is possible to obtain information about the failure mechanism of the bonded samples. It has been stated that the mechanical properties of the bonded samples by the TLP process depend on the type of created phases in the bonding area and their properties. Therefore, the shear tensile strength of joints is highly sensitive to the microstructure of the joint.

The diagram of tensile shear strength of the bonded samples at 1050 °C with holding times of 1, 15, 30, and 45 min is shown in Fig. 7. As it is known, the lowest shear strength is about 140 MPa, which corresponds to the bonded sample at 15 min. According to the microstructure of this joint shown in Fig. 5 (a), it can be seen that the thickness of the η phase layer formed in the joining region is about 16 μm. The increase in the thickness of the η layer and the subsequent increase in the residual stresses at the joining region due to phase mismatch is the reason for the decrease in shear tensile strength. As the time increased to 30 min, as shown in Fig. 5 (b), the thickness of the η layer was not changed much, but the thickness of the isothermal solidification zone increased relative to the time of 15 min. The presence of a nickel-rich solid solution phase in the isothermal solidification zone, which is a ductile phase and has the ability to damp residual stresses, caused the strength of the created joint at a temperature of 1050 °C with a holding time of 30 min to increase as compared with previous times. By increasing the time and reaching 45 min, the thickness of the η phase layer increased again, and therefore the shear tensile strength decreased accordingly. Zidabadinejad et al. [14] also observed such a trend in the shear strength of the created joints between WC-Co and St52 by the TLP process using the Cu interlayer. Of course, it should be mentioned that the maximum shear strength reported by them was around 260 MPa, which is lower than the maximum shear strength of the created joint using the BNi-2 interlayer. The reason for this can be attributed to the higher inherent strength of Ni compared to Cu.

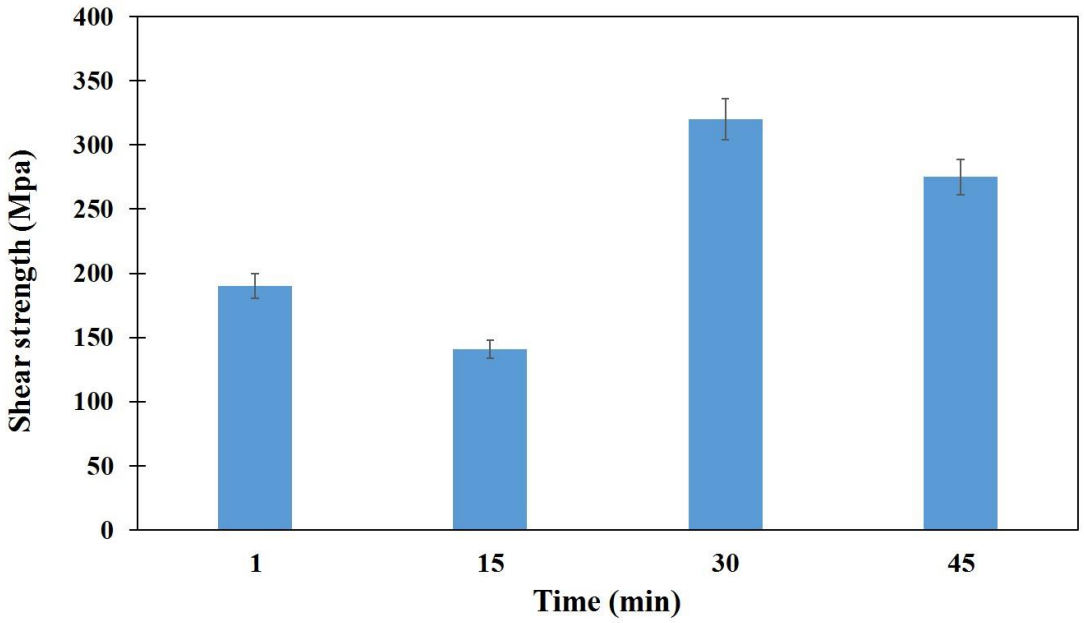

Fig. 7. The changes in the shear tensile strength of the created joint at a constant temperature of 1050 °C at different times.

In order to investigate the mode of failure, the cross-section of the samples subjected to the shear tensile strength test was examined using SEM. Conducting fractography provides information about the failure mechanism and reveals the behavior of joints under the tension. Factors such as the presence or absence of inclusions, impurities, and intermetallic particles or in general, the existence of any heterogeneity in the structure that affects the sliding systems in the material, will affect the way the sample fractures [31].

Fig. 8 shows the fracture surface images of the bonded sample at a temperature of 1050 °C at 1 min using the BNi-2 interlayer. As is clear in these images, a cleavage pattern that indicates brittle failure can be clearly seen in Fig. 8 (a). Also, according to Fig. 8 (b), a dimple-like pattern along with plastic deformation can be observed in some parts of the fracture surface, which indicates ductile fracture. Therefore, according to these images, it can be said that a double brittle-ductile pattern occurred in the failure of this sample. Therefore, it can be stated that the fracture probably occurred at the interface between the isothermal solidification zone and the diffusion-affected zone of the WC-Co base material, where a ductile phase and a relatively brittle phase are located..

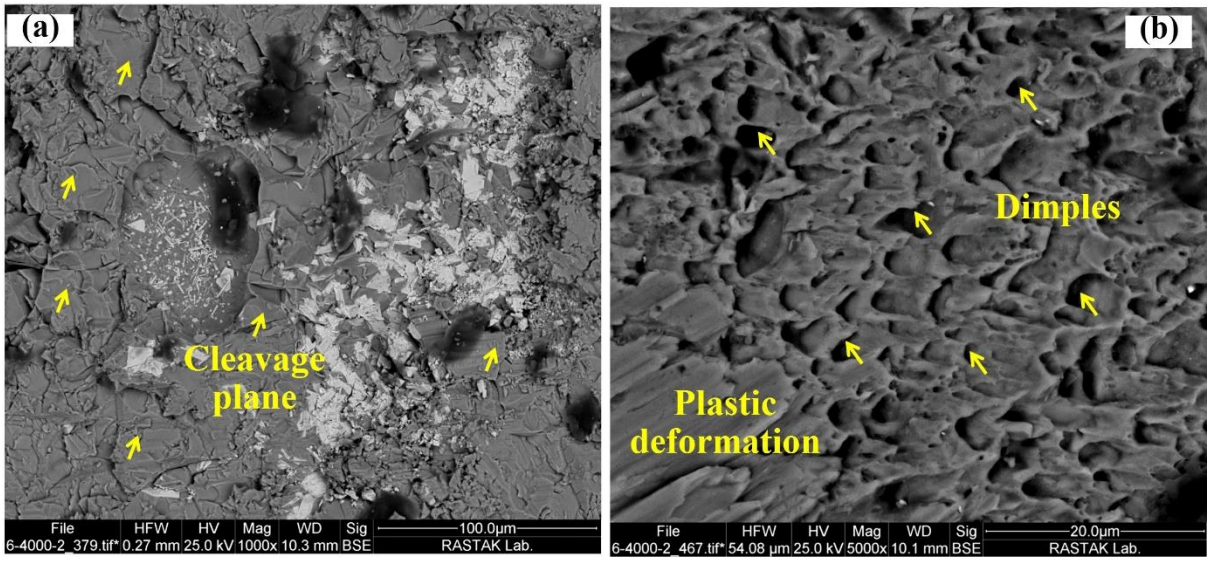

Fig. 8. SEM images of the fracture surface of the bonded sample at temperature of 1050 °C with holding time of 1 min using BNi-2 interlayer.

In order to detect the phases present in the fracture surface, the fracture surfaces were subjected to XRD analysis. The result of this test is shown in Fig. 9. Based on this test, it can be stated that phases such as WC, Co_6W_6C (η phase), Ni_3Fe, and CoWB are present in the fracture surface, which indicates that the fracture in this sample occurred in the diffusion-affected zone of the WC-Co material. Therefore, it can be said that the failure probably started in the diffusion-affected zone of the WC-Co material and then propagated to other areas.

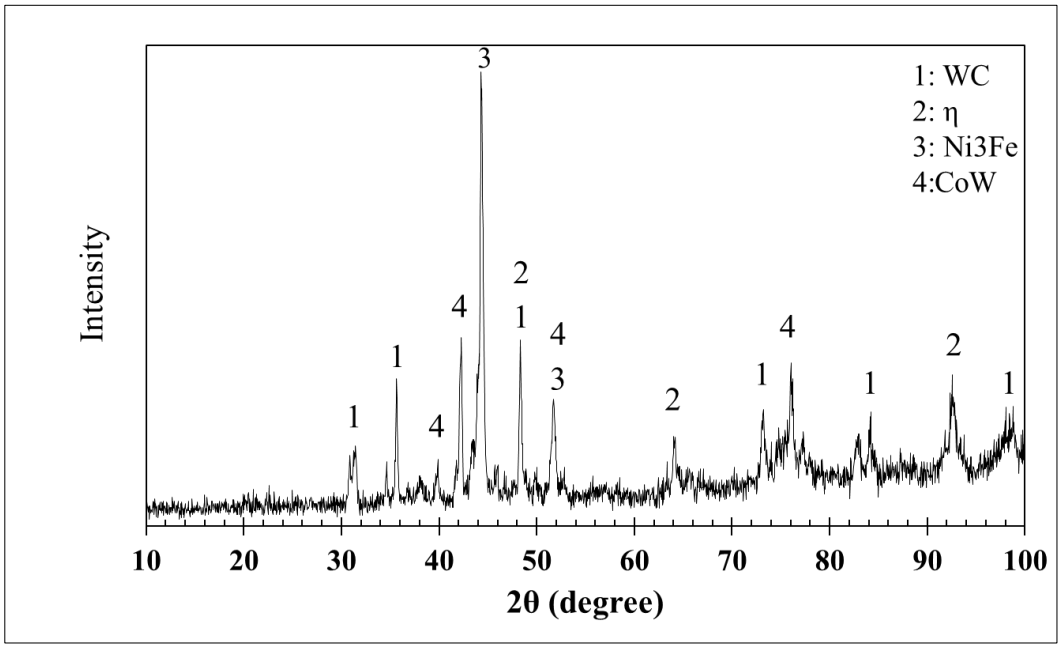

Fig. 9. XRD pattern of the bonded sample at temperature of 1050 °C at 1 min using the BNi-2 interlayer.

By increasing the time up to 45 min, as shown in Fig. 10, the mode of failure is again brittle-ductile in the same way. But it should be mentioned that due to the fact that the dimples are larger than before, more plastic deformation occurred, and this is the reason for the increase in the shear tensile strength of the bonded sample at 45 min (about 275 MPa) compared to the bonded sample at 1 min (about 190 MPa) at a constant temperature of 1050 °C.

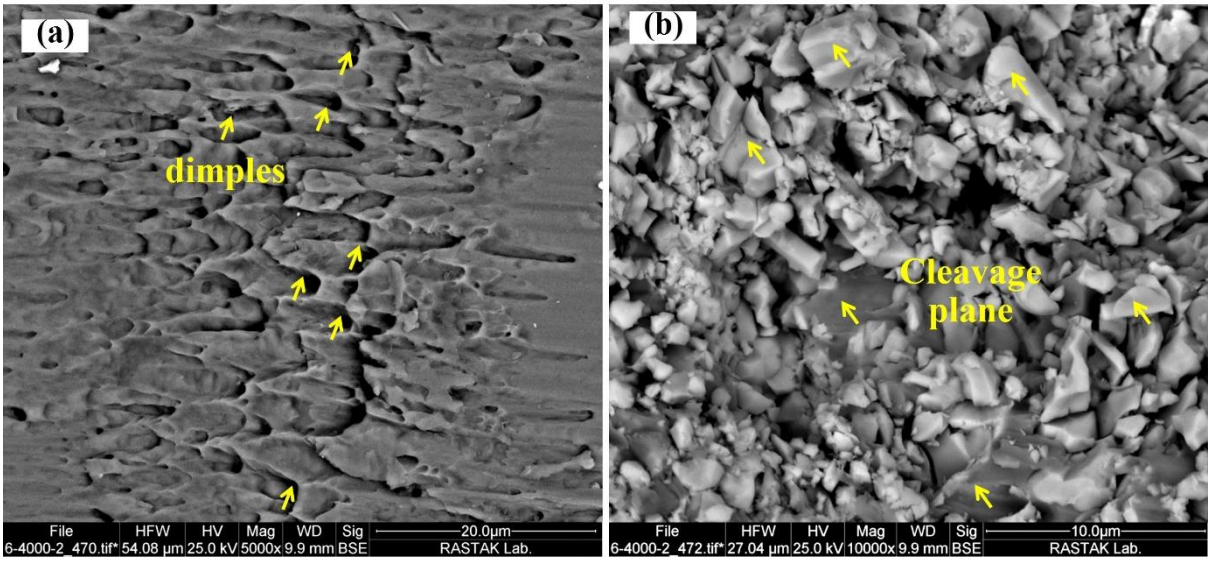

Fig. 10. SEM images of the bonded sample at 1050 °C with bonding time of 45 min using BNi-2 interlayer.

4. Conclusions

The TLP bonding of St52 to WC-Co using 50 µm thickness BNi-2 interlayer at 1050 °C and holding times of 1, 15, 30, and 45 min was investigated, and the following results were obtained:

1- A sound bond between WC-Co and St52 base materials was acquired without any defects or contamination. Based on the microstructural observations, the isothermal solidification zone was created in the central line of the joint.

2- In the isothermal solidification zone, the Ni-base solid solution phase was observed in all samples. Also, the η phase was formed in the diffusion-affected zone of the WC-Co base material.

3- The size of the produced zones in the bonding region depends on the time of the bonding process, and with the change in the bonding time, the size of these zones also changes.

4- The hardness profile for all samples had the same trend, and the maximum hardness was related to the WC-Co base material and the lowest hardness was related to steel base metal.
5- The maximum shear strength was related to the bonded sample at 30 min (about 320 MPa) which was due to the removal and damping of residual stresses by the isothermal solidification zone. The mode of failure in all samples was brittle-ductile.

References

[1] Zhang, X., et al., Vacuum brazing of WC-8Co cemented carbides to carbon steel using pure Cu and Ag-28Cu as filler metal. Journal of Materials Engineering and Performance, 2017. **26**: p. 488-494.

[2] Cheniti, B., et al., Effect of brazing current on microstructure and mechanical behavior of WC-Co/AISI 1020 steel TIG brazed joint. International Journal of Refractory Metals and Hard Materials, 2017. **64**: p. 210-218.

[3] Yu, X.-y., et al., Fiber laser welding of WC-Co to carbon steel using Fe-Ni Invar as interlayer. International Journal of Refractory Metals and Hard Materials, 2016. **56**: p. 76-86.

[4] Chen, G., et al., Electron beam hybrid welding-brazing of WC-Co/40Cr dissimilar materials. Ceramics International, 2019. **45**(6): p. 7821-7829.

[5] Mphasha, N. and D. Whitefield, Microstructure and Mechanical Properties of WC-Co/WC-Co Oxyacetylene Brazed Joints Using Ag-Based Filler Alloy. Journal of Materials Engineering and Performance, 2022. **31**(1): p. 24-36.

[6] Avettand-Fenoel, M.-N., et al., Characterization of WC/12Co cermet–steel dissimilar friction stir welds. Journal of Manufacturing Processes, 2018. **31**: p. 139-155.

[7] Li, S., et al., Microstructural evolution and mechanical properties of diffusion bonding WC-Co cemented carbide to steel using Co and composite Ni/Co interlayers. International Journal of Refractory Metals and Hard Materials, 2022. **103**: p. 105736.

[8] Li, S., et al., Microstructural characteristics and mechanical properties of WC-Co/steel joints diffusion bonded utilizing Ni interlayer. Ceramics International, 2021. **47**(4): p. 4446-4454.

[9] Feng, K., et al., Investigation on diffusion bonding of functionally graded WC–Co/Ni composite and stainless steel. Materials & Design (1980-2015), 2013. **46**: p. 622-626.

[10] Amirnasiri, A. and N. Parvin, Dissimilar diffusion brazing of WC-Co to AISI 4145 steel using RBCuZn-D interlayer. Journal of Manufacturing Processes, 2017. **28**: p. 82-93.

[11] Cai, Q., et al., Microstructure, residual stresses and mechanical properties of diffusion bonded tungsten–steel joint using a V/Cu composite barrier interlayer. International Journal of Refractory Metals and Hard Materials, 2015. **48**: p. 312-317.

[12] Yin, G., et al., Effect of interlayer thickness on the microstructure and strength of WC-Co/Invar/316L steel joints prepared by fibre laser welding. Journal of Materials Processing Technology, 2018. **255**: p. 319-332.

[13] Cheniti, B., et al., Effect of WC-Co cermet positioning and NiCr interlayer on the microstructure and mechanical response of the dissimilar WC-Co/AISI 304 L rotary friction joint. International Journal of Refractory Metals and Hard Materials, 2021. **101**: p. 105653.

[14] Zeidabadinejad, H., et al., Microstructural evolutions and mechanical properties of TLP-bonded WC-Co/St52 with copper interlayer. Welding in the World, 2023: p. 1-11.

[15] Mostaan, H., et al., The effect of microstructure on magnetic properties of TLP bonded Sm 2 Co 17 hard magnets. Applied Physics A, 2020. **126**: p. 1-12.

[16] Pouranvari, M., A. Ekrami, and A. Kokabi, Diffusion induced isothermal solidification during transient liquid phase bonding of cast IN718 superalloy. Canadian Metallurgical Quarterly, 2014. **53**(1): p. 38-46.
[17] Ojo, O., N. Richards, and M. Chaturvedi, Isothermal solidification during transient liquid phase bonding of Inconel 738 superalloy. Science and Technology of Welding and Joining, 2004. **9**(6): p. 532-540.
[18] Pouranvari, M., A. Ekrami, and A. Kokabi, Effect of bonding temperature on microstructure development during TLP bonding of a nickel base superalloy. Journal of Alloys and Compounds, 2009. **469**(1-2): p. 270-275.
[19] Pouranvari, M., A. Ekrami, and A. Kokabi, TLP bonding of cast IN718 nickel based superalloy: process–microstructure–strength characteristics. Materials Science and Engineering: A, 2013. **568**: p. 76-82.
[20] Pouranvari, M., A. Ekrami, and A. Kokabi, Phase transformations during diffusion brazing of IN718/Ni–Cr–B/IN718. Materials Science and Technology, 2013. **29**(8): p. 980-984.
[21] Baharzadeh, E., et al., Properties of IN X-750/BNi-2/SAF 2205 joints formed by transient liquid phase bonding. Journal of Materials Processing Technology, 2019. **274**: p. 116297.
[22] Hawk, C., S. Liu, and S. Kottilingam, Effect of processing parameters on the microstructure and mechanical properties of wide-gap braze repairs on nickel-superalloy René 108. Welding in the World, 2017. **61**: p. 391-404.
[23] Huang, B., et al., Effect of Weld Temperature on Microstructure and Properties of TM52/Q235 Transient Liquid Phase Diffusion-Bonded Joint. Journal of Materials Engineering and Performance, 2022: p. 1-12.
[24] Zhou, X., et al., Transient liquid phase bonding of CLAM/CLAM steels with Ni-based amorphous foil as the interlayer. Materials & Design, 2015. **88**: p. 1321-1325.
[25] Campbell, F., Phase Diagram Applications. Phase Diagrams: Understanding the Basics, Materials Park, Ohio: ASM International, 2012: p. 290-291.
[26] Guo, Y., et al., Effect of temperature on the microstructure and bonding strength of partial transient liquid phase bonded WC–Co/40Cr joints using Ti/Ni/Ti interlayers. International Journal of Refractory Metals and Hard Materials, 2015. **51**: p. 250-257.
[27] Yuan, X., M. Kim, and C. Kang, Effects of boron and silicon on microstructure and isothermal solidification during TLP bonding of a duplex stainless steel using two Ni–Si–B insert alloys. Materials Science and Technology, 2011. **27**(7): p. 1191-1197.
[28] Rhee, B., S. Roh, and D. Kim, Transient liquid phase bonding of nitrogen containing duplex stainless steel UNS S31803 using Ni-Cr-Fe-Si-B insert metal. Materials Transactions, 2003. **44**(5): p. 1014-1023.
[29] Sinclair, C., G. Purdy, and J. Morral, Transient liquid-phase bonding in two-phase ternary systems. Metallurgical and Materials Transactions A, 2000. **31**: p. 1187-1192.
[30] Norouzi, E., et al., Effect of bonding temperature on the microstructure and mechanical properties of Ti-6Al-4V to AISI 304 transient liquid phase bonded joint. Materials & Design, 2016. **99**: p. 543-551.
[31] Hertzberg, R., Deformation and fracture mechanics of engineering materials. NJ: John Wiley & Sons Inc. 1996.